



Cite this: *CrystEngComm*, 2015, 17, 5690

Structural diversity in coordination polymers with a semirigid Lewis acidity ligand: structures and properties†

Yong-Qing Huang,^{*a} Hai-Di Cheng,^a Huai-Ying Chen,^a Yi Wan,^a Cheng-Long Liu,^a Yue Zhao,^{*b} Xin-Feng Xiao^a and Li-Hui Chen^a

Reaction of semirigid Lewis acidity ligand 1-carboxymethylpyridinium-4-carboxylate (*L*) with various salts affords five new coordination networks: two 2D layered coordination polymers $[Ag_2(L)(NO_3)_2] \cdot H_2O$ (2) and $[Pb(L)(NO_3)_2]$ (3), and three 3D metal-organic frameworks $[Cu_4(L)_4(OH)_2Cl_2] \cdot 11.55H_2O$ (1), $[Pb_3(L)_4Br_2(H_2O)_2]$ (4) and $[Pr(L)_2(H_2O)_2(NO_3)_2]$ (5). Complex 1 features a planar tetrานuclear $[Cu_4(\mu_3-OH)_2]^{6+}$ cluster as a 6-connected node, connecting with eight L ligands to generate a tilted α -Po type structure. Compared with 1, 2 possesses a unique 2D double-layered structure with 1D channels, which is composed of (4,4) topological networks pillared by nitrate anions. Complexes 3 and 4 are both made up of 1D chains. 3 is composed of homo-chiral 2_1 helices, which provides a chiral 2D polymeric network, whereas 4 consists of two types of infinite 1D chains linked in a cross-like fashion, which displays a 3D plywood-like structure. Complex 5 consists of 4-connected metal nodes, which exhibits a 3-fold interpenetrating 3D diamondoid framework. The results suggest that the semirigid *L* ligand adopting different coordination modes plays important roles in determining the final structures of complexes 1–5. Moreover, complexes 3 and 5 with an acentric space group show modest powder second-harmonic-generation (SHG) efficiency at room temperature. Based on the Lewis acidity of the pyridinium unit of ligand *L*, complexes 1–5 were also used as catalysts for aza-Diels–Alder reaction.

Received 7th April 2015,
Accepted 12th June 2015

DOI: 10.1039/c5ce00677e
www.rsc.org/crystengcomm

Introduction

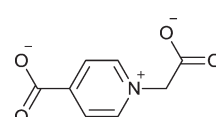
Metal–organic hybrid coordination polymer materials have recently been spurred by their potential applications in nonlinear optics,¹ luminescence,² gas storage,³ adsorption separation,⁴ heterogeneous catalysis⁵ and many other areas.⁶ Among them, catalysis is one of the most promising applications of such materials. Generally speaking, the self-assembly of a highly organized structure depends mainly on the metal-ion-directed geometry and pre-designed organic bridging ligand with specific conformation besides crystallization conditions.⁷ In contrast to limited metal ions/clusters as the nodes, theoretically numerous organic spacers play more crucial roles in the construction of coordination networks, because the flexibility of the organic backbone,

conformational preference and symmetry of organic ligands can lead to a remarkable series of materials bearing various structures and structure-driven properties. Among them, the semirigid ligands have demonstrated their efficiency as building blocks in the construction of novel coordination polymers with specific structures.⁸ In contrast to rigid ligands with fixed conformation and flexible ligands with changing configuration in the assembly of target coordination polymers, the semirigid ligands combine the advantages of both. In other words, the semirigid ligands can keep a certain shape and, meanwhile, timely adjust their partial configuration to enhance the structural variation. On the other hand, in the past investigations, carboxylate ligands, especially with specific conformation, have been widely used due to their various coordination modes and good coordination capacities.⁹ Based on the above reason, we selected and synthesized *L*-shaped semirigid Lewis acidity ligand 1-carboxymethylpyridinium-4-carboxylate (*L*, Scheme 1), which can twist around the

^a State Key Laboratory of Mining Disaster Prevention and Control Co-founded by Shandong Province and the Ministry of Science and Technology, Shandong University of Science and Technology, Qingdao 266590, China. E-mail: yqhuangskd@163.com

^b State Key Laboratory of Coordination Chemistry, School of Chemistry and Chemical engineering, Nanjing National Laboratory of Microstructures, Nanjing University, Nanjing 210093, China

† Electronic supplementary information (ESI) available: IR spectra, TGA curves, PXRD patterns, additional structural figures and hydrogen-bonding data, and X-ray crystallographic files for compounds 1–5 in CIF format. CCDC 1008931, 1008932, 1008934–1008936. See DOI: 10.1039/c5ce00677e



Scheme 1 Structure of the ligand *L*.

secondary carbon atom at different angles to adapt different coordination environments.¹⁰ In addition, the L ligand belongs to the zwitterionic carboxylate ligand, referred to as a betaine derivative or dipolar ion compound, which has a permanent weak Lewis acidity site and can be a candidate for the Lewis acid catalytic reaction.¹¹ Herein, we report the synthesis, crystal structures and properties of five new complexes, namely, $[\text{Cu}_4(\text{L})_4(\text{OH})_2\text{Cl}_2]\cdot11.55\text{H}_2\text{O}$ (1), $[\text{Ag}_2(\text{L})(\text{NO}_3)]\cdot\text{H}_2\text{O}$ (2), $[\text{Pb}(\text{L})(\text{NO}_3)]$ (3), $[\text{Pb}_3(\text{L})_4\text{Br}_2(\text{H}_2\text{O})_2]$ (4) and $[\text{Pr}(\text{L})_2(\text{H}_2\text{O})_2(\text{NO}_3)]$ (5).

Experimental

Materials and methods

All materials were of reagent grade, obtained from commercial sources and used without further purification. Solvents were dried by standard procedures. The ligand L was prepared according to the method of Kass.¹² Elemental analyses (C, H, N) were carried out using a Perkin-Elmer 240C elemental analyser. Infrared spectra were recorded in the range of 4000–400 cm⁻¹ with a Nicolet 380 FT-IR spectrometer using KBr pellets. Powder X-ray diffraction (PXRD) patterns were measured at ambient temperature using a Rigaku Ultima IV diffractometer for complexes 1, 2, 4 and 5 and Shimadzu XRD-6000 X-ray diffractometer for complex 3 with graphite monochromatic Cu K α radiation ($\lambda = 0.15418$ nm) at 40 kV and 40 mA. Simulated powder patterns were based on single crystal data and calculated using the Mercury software.¹³ Thermogravimetric analyses (TGA) were performed using a Mettler-Toledo thermal analyzer under nitrogen atmosphere with a heating rate of 10 °C min⁻¹. The second-order non-linear optical (NLO) intensity was estimated by measuring powder samples relative to urea. A pulsed Q-switched Nd:YAG laser at a wavelength of 1064 nm was used to generate a SHG signal from powder samples. The backscattered SHG light was collected with a spherical concave mirror and passed through a filter that transmits only 532 nm radiation. ¹H NMR spectra were recorded on a Bruker DRX 400 NMR spectrometer.

Synthesis of $[\text{Cu}_4(\text{L})_4(\text{OH})_2\text{Cl}_2]\cdot11.55\text{H}_2\text{O}$ (1)

A mixture of $\text{CuCl}_2\cdot2\text{H}_2\text{O}$ (34.1 mg, 0.2 mmol) and L (22.0 mg, 0.1 mmol) in water (7 mL) was stirred for 20 min at ambient temperature. Three weeks later, blue crystals were obtained by slow diffusion of acetone into the clear filtrate. Yield: 43%. Anal. calcd for $\text{C}_{32}\text{H}_{49.10}\text{Cl}_2\text{Cu}_4\text{N}_4\text{O}_{29.55}$: C, 29.85; H, 3.84; N, 4.35. Found: C, 29.95; H, 3.61; N, 4.12. IR (KBr, cm⁻¹): 3524 (m), 3474 (m), 3050 (s), 1665 (vs), 1643 (vs), 1565 (s), 1458 (m), 1374 (vs), 1347 (vs), 1291 (s), 1189 (m), 822 (m), 725 (m), 668 (m), 587 (w), 520 (w).

Synthesis of $[\text{Ag}_2(\text{L})(\text{NO}_3)]\cdot\text{H}_2\text{O}$ (2)

AgNO_3 (68.0 mg, 0.4 mmol) and L (44.0 mg, 0.2 mmol) were mixed in water (3 mL), then aqueous ammonia (1 mol·L⁻¹) was added dropwise until the pH value of the solution was

11. After filtration, the solution was left to stand in a dark place. Six weeks later, the rodlike crystals suitable for X-ray diffraction were obtained. Yield: 26%. Anal. calcd for $\text{C}_8\text{H}_8\text{Ag}_2\text{N}_2\text{O}_8$: C, 20.19; H, 1.69; N, 5.89. Found: C, 20.34; H, 1.65; N, 5.92. IR (KBr, cm⁻¹): 3376 (s), 3047 (s), 1629 (vs), 1560 (s), 1375 (vs), 1190 (m), 910 (w), 820 (s), 786 (m), 718 (s), 581 (w).

Synthesis of $[\text{Pb}(\text{L})(\text{NO}_3)]$ (3)

A buffer layer of a 5 mL solution of methanol–water (2:3) was carefully layered over a solution of $\text{Pb}(\text{NO}_3)_2\cdot4\text{H}_2\text{O}$ (80.6 mg, 0.2 mmol) in water (3 mL). Then a 6 mL methanol–water (2:1) solution of L (22.0 mg, 0.1 mmol) was layered over the buffer layer. The solution was left to stand for 2 weeks at room temperature, and colorless block-like crystals appeared in 45% yield. Anal. calcd for $\text{C}_8\text{H}_6\text{PbN}_2\text{O}_7$: C, 21.38; H, 1.35; N, 6.23. Found: C, 21.43; H, 1.44; N, 6.21. IR (KBr, cm⁻¹): 3349 (m), 3115 (m), 3047 (m), 2999 (m), 1609 (s), 1560 (s), 1369 (s), 1293 (s), 1033 (w), 910 (w), 820 (m), 711 (m), 657 (w).

Synthesis of $[\text{Pb}_3(\text{L})_4\text{Br}_2(\text{H}_2\text{O})_2]$ (4)

A buffer layer of a 5 mL solution of methanol–water (2:3) was carefully layered over a solution of $\text{Pb}(\text{NO}_3)_2\cdot4\text{H}_2\text{O}$ (80.6 mg, 0.2 mmol) in water (3 mL). Then a 6 mL methanol–water (2:1) solution of L (22.0 mg, 0.1 mmol) and KBr (11.9 mg, 0.1 mmol) was layered over the buffer layer. The solution was left to stand for two weeks at room temperature, and colorless needle-like crystals appeared in 75% yield. Anal. calcd for $\text{C}_{32}\text{H}_{28}\text{Br}_2\text{Pb}_3\text{N}_4\text{O}_{18}$: C, 24.99; H, 1.84; N, 3.64. Found: C, 25.07; H, 1.66; N, 3.79. IR (KBr, cm⁻¹): 3349 (w), 3047 (m), 1615 (vs), 1560 (vs), 1375 (vs), 1279 (s), 910 (w), 820 (m), 704 (m), 657 (w).

Synthesis of $[\text{Pr}(\text{L})_2(\text{H}_2\text{O})_2(\text{NO}_3)]$ (5)

A mixture of $\text{Pr}(\text{NO}_3)_2\cdot6\text{H}_2\text{O}$ (87.0 mg, 0.2 mmol) and L (44.0 mg, 0.2 mmol) in water (4 mL) was stirred for 20 min at ambient temperature. Three weeks later, crystals suitable for X-ray diffraction were obtained by slow diffusion of acetone into the clear filtrate. Yield: 33%. Anal. calcd for $\text{C}_{16}\text{H}_{16}\text{PrN}_3\text{O}_{13}$: C, 45.51; H, 4.62; N, 8.38. Found: C, 45.72; H, 4.60; N, 8.15. IR (KBr, cm⁻¹): 3438 (s), 3118 (s), 3056 (s), 1643 (vs.), 1617 (vs), 1567 (s), 1466 (s), 1369 (vs), 1314 (s), 1213 (w), 1033 (w), 823 (w), 713 (m), 649 (m).

Typical procedure for catalytic activity studies

N-Benzylideneaniline (0.2 mmol), complex catalysts with a 0.02 mmol (10 mol%) L ligand, Danishefsky's diene (0.22 mmol, 42.8 μL) and 2 mL of MeCN were introduced into a dry Schlenk flask under nitrogen. After stirring for 24 h at room temperature, the mixture was quenched by addition of a saturated solution of potassium hydrogen carbonate (2 mL) and extracted with ethyl acetate (3×5 mL). The organic layer was dried over anhydrous Na_2SO_4 and distilled off under reduced pressure. TLC (PE-EtOAc, 1:2) gave the desired product.

X-Ray crystallography

The diffraction data were collected using a Bruker Smart Apex CCD diffractometer for complexes **1**, **2**, **4** and **5** and an Agilent Xcalibur Eos Gemini diffractometer for complex **5** with graphite-monochromated Mo K α radiation ($\lambda = 0.71073 \text{ \AA}$). Empirical absorption corrections were applied to the data using the multi-scan program SADABS¹⁴ for **1**, **2**, **3** and **4** and CrysAlis PRO¹⁵ for **5**. The structures were solved by the direct method (SHELXS-97)¹⁶ and refined by the full-matrix least-square method on F^2 using the SHELXL-97 program.¹⁷ The coordinates of the non-hydrogen atoms were refined anisotropically. All hydrogen atoms were inserted at the ideal positions and refined using a riding model isotropically except for the H atoms of H₂O molecules. The water H atoms in **2**, **4** and **5** were located in a difference map and refined with distance restraints of O–H = 0.82(1) \AA , whereas the water H atoms in **1** had not been added. All calculations were carried out using the SHELXTL crystallographic software package.¹⁸ Details of the crystal parameters, data collections and refinement for **1**–**5** are summarized in Table 1. Selected bond lengths and angles with their estimated standard deviations are given in Table 2. Hydrogen-bonding data are listed in Table S1.[†]

Results and discussion

Structure of [Cu₄(L)₄(OH)₂Cl₂]·11.55H₂O (1)

Compound **1** crystallizes in the monoclinic $P2_1/n$ space group (Table 1) and possesses a tilted α -Po type (pcu: 4¹²·6³) 3D network with the tetranuclear $[\text{Cu}_4(\mu_3\text{-OH})_2]^{6+}$ cores as six-connected nodes. Fig. 1 shows that two crystallographically

independent Cu(II) centers exist in the asymmetric unit of **1**. Each Cu1 ion is in a significantly distorted square pyramidal sphere ($\tau = 0.335$),¹⁹ being coordinated by a Cl atom and two O atoms from two different L ligands as well as two O atoms from two different hydroxo bridges. The bond distances and bond angles around Cu1 range from 1.934(2) to 2.264(14) \AA and 78.38(9) $^\circ$ to 168.77(9) $^\circ$, respectively, as listed in Table 2. Compared to the Cu1 center, each Cu2 center adopts a pentacoordinated regular tetragonal pyramid geometry ($\tau = 0.129$) with four L ligands and one hydroxo bridge. The average equatorial and axial bond lengths around Cu2 are 1.964 and 2.287 \AA , respectively, implying that the Jahn–Teller distortion happens around the Cu2 center.²⁰ Moreover, the Cu2 ion is displaced out of the basal plane defined by O2, O7, O9 and O5A toward the apical O4A atom with a displacement of 0.073 \AA .

The structure of **1** features the tetranuclear copper cores as six-connected topological nodes. As displayed in Fig. 2, the $[\text{Cu}_4(\mu_3\text{-OH})_2]^{6+}$ core is enveloped by eight bridging L ligands, in which the intermetallic distances are short (Cu1–Cu2 3.1990(18) \AA , Cu1–Cu2A 3.3718(14) \AA , Cu1–Cu1A 3.0230(13) \AA , and Cu2–Cu2A 5.8367(26) \AA), similar to that of the reported compound $[\text{Cu}_4(\text{L})_4(\text{OH})_2(\text{H}_2\text{O})_2](\text{NO}_3)_2 \cdot 3\text{H}_2\text{O}$.¹⁰ Obviously, two $\mu_3\text{-O}$ atoms are situated in the opposite side of the rhombus Cu₄ plane with a deviation of 0.707 \AA , so the geometry of the $[\text{Cu}_4(\mu_3\text{-OH})_2]^{6+}$ core can also be regarded as the combination of two edge-shared (Cu–Cu1A) tetrahedra with a Cu₃O vertex set. On the other hand, the L ligands show two types of distinctly different bridging modes: one serves as a bis-bidentate μ_4 -bridging ligand to connect four Cu(II) ions, in which two carboxyl groups both take the

Table 1 Crystallographic data and refinement parameters for **1**–**5**^a

| Compounds | 1 | 2 | 3 | 4 | 5 |
|---|--|---|---|--|--|
| Empirical formula | C ₃₂ H _{49.10} Cl ₂ Cu ₄ N ₄ O _{29.55} | C ₈ H ₈ Ag ₂ N ₂ O ₈ | C ₈ H ₆ PbN ₂ O ₇ | C ₃₂ H ₂₈ Br ₂ Pb ₃ N ₄ O ₁₈ | C ₁₆ H ₁₆ PrN ₃ O ₁₃ |
| Formula weight | 1287.63 | 475.90 | 449.34 | 1537.97 | 599.23 |
| Crystal system | Monoclinic | Monoclinic | Orthorhombic | Monoclinic | Orthorhombic |
| Space group | $P2_1/n$ | $P2_1/n$ | $P2_12_12_1$ | $C2/c$ | $Fdd2$ |
| <i>a</i> (\AA) | 8.697(6) | 12.0276(11) | 4.5139(3) | 24.044(3) | 10.5744(5) |
| <i>b</i> (\AA) | 25.057(17) | 5.2148(4) A | 11.3181(7) | 10.7102(14) | 39.183(3) |
| <i>c</i> (\AA) | 11.638(8) | 17.8366(16) | 20.4554(14) | 16.138(2) | 9.2768(5) |
| α ($^\circ$) | 90 | 90 | 90 | 90 | 90 |
| β ($^\circ$) | 104.010(10) | 91.7730(10) | 90 | 110.264(2) | 90 |
| γ ($^\circ$) | 90 | 90 | 90 | 90 | 90 |
| <i>V</i> (\AA^3) | 2460(3) | 1118.20(17) | 1045.0(12) | 3898.4(9) | 3843.7(4) |
| <i>Z</i> | 2 | 4 | 4 | 4 | 8 |
| <i>D</i> _{calc} (g cm^{-3}) | 1.738 | 2.827 | 2.856 | 2.620 | 2.071 |
| μ (mm^{-1}) | 1.912 | 3.547 | 16.176 | 15.057 | 2.617 |
| <i>T</i> (K) | 296 | 296 | 296 | 296 | 108 |
| <i>F</i> (000) | 1311 | 912 | 824 | 2832 | 2368 |
| θ_{\max} ($^\circ$) | 55 | 51 | 56.8 | 50 | 55 |
| Independent reflections | 5654 | 2044 | 2596 | 3389 | 2140 |
| Data/restraints/parameters | 5654/0/326 | 2044/2/188 | 2596/0/163 | 3389/2/273 | 2140/3/159 |
| <i>R</i> _{int} | 0.0253 | 0.0333 | 0.0553 | 0.0492 | 0.0301 |
| Goodness-of-fit on F^2 | 1.027 | 1.064 | 0.953 | 1.043 | 1.095 |
| <i>R</i> ₁ , w <i>R</i> ₂ ^a ($I > 2\sigma(I)$) | 0.0371, 0.1056 | 0.0388, 0.0990 | 0.0327, 0.0739 | 0.0658, 0.2075 | 0.0249, 0.0617 |
| <i>R</i> ₁ , ^a w <i>R</i> ₂ (all data) | 0.0458, 0.1098 | 0.0404, 0.1005 | 0.0363, 0.0762 | 0.0735, 0.2161 | 0.0260, 0.0625 |

^a $R_1 = \sum |F_O| - |F_C| / \sum |F_O|$; $wR_2 = \{\sum [w(F_O^2 - F_C^2)^2] / \sum [w(F_O^2)]\}^{1/2}$.

Table 2 Selected bond distances (\AA) and angles ($^\circ$) for 1–5^a

| 1 | | | |
|--|-------------|---|-------------|
| Cu(1)–O(3) ^{#1} | 1.934(2) | Cu(1)–O(9) | 1.957(2) |
| Cu(1)–O(9) ^{#2} | 2.020(2) | Cu(1)–Cl(1) | 2.2642(14) |
| Cu(1)–O(1) | 2.360(2) | Cu(1)–Cu(1) ^{#2} | 3.0229(14) |
| Cu(2)–O(2) | 1.952(2) | Cu(2)–O(7) | 1.957(2) |
| Cu(2)–O(5) ^{#3} | 1.971(2) | Cu(2)–O(9) | 1.976(2) |
| Cu(2)–O(4) ^{#4} | 2.286(2) | | |
| O(3) ^{#1} –Cu(1)–O(9) | 168.77(9) | O(3) ^{#1} –Cu(1)–O(9) ^{#2} | 95.90(8) |
| O(9)–Cu(1)–O(9) ^{#2} | 81.08(8) | O(3) ^{#1} –Cu(1)–Cl(1) | 93.57(8) |
| O(9)–Cu(1)–Cl(1) | 94.54(6) | O(9) ^{#2} –Cu(1)–Cl(1) | 148.68(6) |
| O(3) ^{#1} –Cu(1)–O(1) | 78.38(9) | O(9)–Cu(1)–O(1) | 91.01(8) |
| O(9) ^{#2} –Cu(1)–O(1) | 94.21(8) | Cl(1)–Cu(1)–O(1) | 116.95(7) |
| O(3) ^{#1} –Cu(1)–Cu(1) ^{#2} | 134.72(8) | O(9)–Cu(1)–Cu(1) ^{#2} | 41.33(6) |
| O(9) ^{#2} –Cu(1)–Cu(1) ^{#2} | 39.75(5) | Cl(1)–Cu(1)–Cu(1) ^{#2} | 128.48(4) |
| O(1)–Cu(1)–Cu(1) ^{#2} | 93.47(6) | O(2)–Cu(2)–O(7) | 171.08(9) |
| O(2)–Cu(2)–O(5) ^{#3} | 89.04(10) | O(7)–Cu(2)–O(5) ^{#3} | 86.95(10) |
| O(2)–Cu(2)–O(9) | 89.91(9) | O(7)–Cu(2)–O(9) | 94.01(9) |
| O(5) ^{#3} –Cu(2)–O(9) | 178.84(8) | O(2)–Cu(2)–O(4) ^{#4} | 98.66(10) |
| O(7)–Cu(2)–O(4) ^{#4} | 89.06(11) | O(5) ^{#3} –Cu(2)–O(4) ^{#4} | 86.54(8) |
| O(9)–Cu(2)–O(4) ^{#4} | 94.11(8) | | |
| 2 | | | |
| Ag(1)–O(2) ^{#5} | 2.266(3) | Ag(1)–O(3) ^{#6} | 2.405(3) |
| Ag(1)–O(5) | 2.561(6) | Ag(1)–Ag(2) | 2.8367(6) |
| Ag(1)–Ag(2) ^{#6} | 3.2073(6) | Ag(2)–O(1) ^{#5} | 2.343(3) |
| Ag(2)–O(4) ^{#6} | 2.359(4) | Ag(2)–O(3) | 2.382(3) |
| Ag(2)–O(7) ^{#7} | 2.455(5) | Ag(2)–O(5) ^{#8} | 2.529(4) |
| Ag(2)–Ag(1) ^{#8} | 3.2073(6) | | |
| O(2) ^{#5} –Ag(1)–O(3) ^{#6} | 136.23(13) | O(2) ^{#5} –Ag(1)–O(5) | 132.26(13) |
| O(3) ^{#6} –Ag(1)–O(5) | 88.21(12) | O(2) ^{#5} –Ag(1)–Ag(2) | 83.86(9) |
| O(3) ^{#6} –Ag(1)–Ag(2) | 71.75(8) | O(5)–Ag(1)–Ag(2) | 136.21(10) |
| O(2) ^{#5} –Ag(1)–Ag(2) ^{#6} | 142.20(9) | O(3) ^{#6} –Ag(1)–Ag(2) ^{#6} | 47.64(8) |
| O(5)–Ag(1)–Ag(2) ^{#6} | 50.50(10) | Ag(2)–Ag(1)–Ag(2) ^{#6} | 119.142(19) |
| O(1) ^{#5} –Ag(2)–O(4) ^{#6} | 103.54(13) | O(1) ^{#5} –Ag(2)–O(3) | 87.20(12) |
| O(4) ^{#6} –Ag(2)–O(3) | 102.30(12) | O(1) ^{#5} –Ag(2)–O(7) ^{#7} | 168.47(15) |
| O(4) ^{#6} –Ag(2)–O(7) ^{#7} | 84.71(19) | O(3)–Ag(2)–O(7) ^{#7} | 99.02(14) |
| O(1) ^{#5} –Ag(2)–O(5) ^{#8} | 79.82(14) | O(4) ^{#6} –Ag(2)–O(5) ^{#8} | 167.85(17) |
| O(3)–Ag(2)–O(5) ^{#8} | 89.46(16) | O(7) ^{#7} –Ag(2)–O(5) ^{#8} | 90.48(19) |
| O(1) ^{#5} –Ag(2)–Ag(1) | 80.05(9) | O(4) ^{#6} –Ag(2)–Ag(1) | 85.60(9) |
| O(3)–Ag(2)–Ag(1) | 166.33(8) | O(7) ^{#7} –Ag(2)–Ag(1) | 92.75(11) |
| O(5) ^{#8} –Ag(2)–Ag(1) | 83.49(14) | O(1) ^{#5} –Ag(2)–Ag(1) ^{#8} | 56.46(9) |
| O(4) ^{#6} –Ag(2)–Ag(1) ^{#8} | 140.04(9) | O(3)–Ag(2)–Ag(1) ^{#8} | 48.23(7) |
| O(7) ^{#7} –Ag(2)–Ag(1) ^{#8} | 121.44(16) | O(5) ^{#8} –Ag(2)–Ag(1) ^{#8} | 51.39(14) |
| Ag(1)–Ag(2)–Ag(1) ^{#8} | 119.142(19) | | |
| 3 | | | |
| Pb(1)–O(2) ^{#9} | 2.437(5) | Pb(1)–O(3) ^{#10} | 2.566(6) |
| Pb(1)–O(4) | 2.564(7) | Pb(1)–O(1) ^{#11} | 2.649(6) |
| Pb(1)–O(6) | 2.692(8) | | |
| O(2) ^{#9} –Pb(1)–O(3) ^{#10} | 75.0(2) | O(2) ^{#9} –Pb(1)–O(4) | 76.6(2) |
| O(3) ^{#10} –Pb(1)–O(4) | 81.2(2) | O(2) ^{#9} –Pb(1)–O(1) ^{#11} | 74.04(19) |
| O(3) ^{#10} –Pb(1)–O(1) ^{#11} | 84.08(19) | O(4)–Pb(1)–O(1) ^{#11} | 149.68(19) |
| O(2) ^{#9} –Pb(1)–O(6) | 88.4(2) | O(3) ^{#10} –Pb(1)–O(6) | 155.8(2) |
| O(4)–Pb(1)–O(6) | 112.3(2) | O(1) ^{#11} –Pb(1)–O(6) | 74.41(19) |
| 4 | | | |
| Pb(1)–O(6) | 2.637(10) | Pb(1)–O(6) ^{#12} | 2.637(10) |
| Pb(1)–O(8) ^{#13} | 2.727(9) | Pb(1)–O(8) ^{#14} | 2.727(9) |
| Pb(1)–Br(1) ^{#12} | 2.9175(13) | Pb(1)–Br(1) | 2.9175(13) |
| Pb(2)–O(2) ^{#15} | 2.515(11) | Pb(2)–O(4) | 2.636(9) |
| Pb(2)–O(3) | 2.639(9) | Pb(2)–O(6) | 2.640(8) |
| Pb(2)–O(1W) | 2.693(11) | Pb(2)–O(4) ^{#16} | 2.713(9) |
| O(6)–Pb(1)–O(6) ^{#12} | 149.7(4) | O(6)–Pb(1)–O(8) ^{#13} | 76.3(3) |
| O(6) ^{#12} –Pb(1)–O(8) ^{#13} | 127.5(3) | O(6)–Pb(1)–O(8) ^{#14} | 127.5(3) |
| O(6) ^{#12} –Pb(1)–O(8) ^{#14} | 76.3(3) | O(8) ^{#13} –Pb(1)–O(8) ^{#14} | 89.6(4) |
| O(6)–Pb(1)–Br(1) ^{#12} | 74.73(18) | O(6) ^{#12} –Pb(1)–Br(1) ^{#12} | 85.3(2) |

Table 2 (continued)

| 4 | | | |
|---|------------|---|------------|
| O(8) ^{#13} -Pb(1)-Br(1) ^{#12} | 90.9(2) | O(8) ^{#14} -Pb(1)-Br(1) ^{#12} | 157.1(2) |
| O(6)-Pb(1)-Br(1) | 85.3(2) | O(6) ^{#12} -Pb(1)-Br(1) | 74.73(18) |
| O(8) ^{#13} -Pb(1)-Br(1) | 157.1(2) | O(8) ^{#14} -Pb(1)-Br(1) | 90.9(2) |
| Br(1) ^{#12} -Pb(1)-Br(1) | 97.49(5) | O(2) ^{#15} -Pb(2)-O(4) | 76.7(3) |
| O(2) ^{#15} -Pb(2)-O(3) | 72.3(3) | O(4)-Pb(2)-O(3) | 49.7(3) |
| O(2) ^{#15} -Pb(2)-O(6) | 85.8(3) | O(4)-Pb(2)-O(6) | 130.5(3) |
| O(3)-Pb(2)-O(6) | 81.0(3) | O(2) ^{#15} -Pb(2)-O(1W) | 143.4(3) |
| O(4)-Pb(2)-O(1W) | 76.8(3) | O(3)-Pb(2)-O(1W) | 107.7(3) |
| O(6)-Pb(2)-O(1W) | 130.8(3) | O(2) ^{#15} -Pb(2)-O(4) ^{#16} | 77.4(3) |
| O(4)-Pb(2)-O(4) ^{#16} | 70.3(3) | O(3)-Pb(2)-O(4) ^{#16} | 116.9(3) |
| O(6)-Pb(2)-O(4) ^{#16} | 149.3(3) | O(1W)-Pb(2)-O(4) ^{#16} | 70.3(3) |
| 5 | | | |
| Pr(1)-O(3) | 2.414(3) | Pr(1)-O(3) ^{#17} | 2.414(3) |
| Pr(1)-O(1) ^{#18} | 2.446(3) | Pr(1)-O(1) ^{#19} | 2.446(3) |
| Pr(1)-O(1W) ^{#17} | 2.446(3) | Pr(1)-O(1W) | 2.446(3) |
| Pr(1)-O(5) ^{#17} | 2.639(3) | Pr(1)-O(5) | 2.639(3) |
| O(3)-Pr(1)-O(3) ^{#17} | 138.42(15) | O(3)-Pr(1)-O(1) ^{#18} | 77.42(10) |
| O(3) ^{#17} -Pr(1)-O(1) ^{#18} | 141.45(10) | O(3)-Pr(1)-O(1) ^{#19} | 141.46(10) |
| O(3) ^{#17} -Pr(1)-O(1) ^{#19} | 77.42(10) | O(1) ^{#18} -Pr(1)-O(1) ^{#19} | 74.70(13) |
| O(3)-Pr(1)-O(1W) ^{#17} | 98.46(11) | O(3) ^{#17} -Pr(1)-O(1W) ^{#17} | 85.79(11) |
| O(1) ^{#18} -Pr(1)-O(1W) ^{#17} | 72.40(9) | O(1) ^{#19} -Pr(1)-O(1W) ^{#17} | 97.89(9) |
| O(3)-Pr(1)-O(1W) | 85.79(11) | O(3) ^{#17} -Pr(1)-O(1W) | 98.46(11) |
| O(1) ^{#18} -Pr(1)-O(1W) | 97.89(9) | O(1) ^{#19} -Pr(1)-O(1W) | 72.40(9) |
| O(1W) ^{#17} -Pr(1)-O(1W) | 168.08(14) | O(3)-Pr(1)-O(5) ^{#17} | 72.34(9) |
| O(3) ^{#17} -Pr(1)-O(5) ^{#17} | 69.93(9) | O(1) ^{#18} -Pr(1)-O(5) ^{#17} | 148.60(8) |
| O(1) ^{#19} -Pr(1)-O(5) ^{#17} | 126.46(9) | O(1W) ^{#17} -Pr(1)-O(5) ^{#17} | 119.97(10) |
| O(1W)-Pr(1)-O(5) ^{#17} | 71.91(10) | O(3)-Pr(1)-O(5) | 69.93(9) |
| O(3) ^{#17} -Pr(1)-O(5) | 72.34(9) | O(1) ^{#18} -Pr(1)-O(5) | 126.46(9) |
| O(1) ^{#19} -Pr(1)-O(5) | 148.60(8) | O(1W) ^{#17} -Pr(1)-O(5) | 71.91(10) |
| O(1W)-Pr(1)-O(5) | 119.97(10) | O(5) ^{#17} -Pr(1)-O(5) | 48.81(13) |

^a Symmetry transformations used to generate equivalent atoms: #1 -x + 1, -y, -z + 2; #2 -x + 1, -y, -z + 1; #3 x - 1/2, -y + 1/2, z + 1/2; #4 x, y, z - 1; #5 x + 1/2, -y + 1/2, z - 1/2; #6 x, y + 1, z; #7 -x + 2, -y + 2, -z + 1; #8 -, y - 1, z; #9 -x, y-1/2, -z + 3/2; #10 x + 1, y, z; #11 -x + 1, y - 1/2, -z + 3/2; #12 -x, y, -z + 1/2; #13 -x, -y + 2, -z + 1; #14 x, -y + 2, z - 1/2; #15 x, y + 1, z; #16 -x + 1/2, -y + 5/2, -z + 1; #17 -x + 1/2, -y + 1/2, z; #18 x + 1/4, -y + 1/4, z - 3/4; #19 -x + 1/4, y + 1/4, z - 3/4.

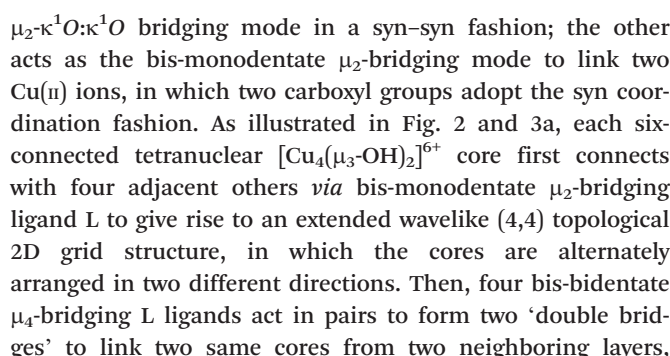


Fig. 1 View of the Cu(II) coordination environment observed in 1. The hydrogen atoms and guest water molecules were omitted for clarity.

leading to an infinite chain (Fig. 3b). The center-to-center distance between two cores in the 1D chain is 11.6380(77) Å,

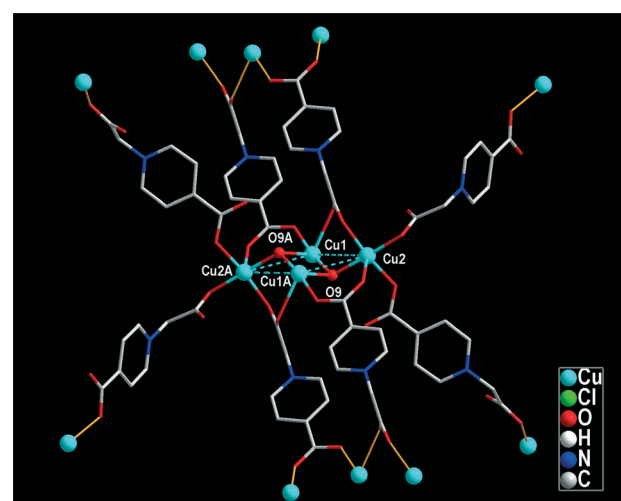


Fig. 2 View of the tetranuclear Cu(II) core, showing the coordination modes of the hydroxo bridge and L ligand. The hydrogen atoms and chloride ions were omitted for clarity.

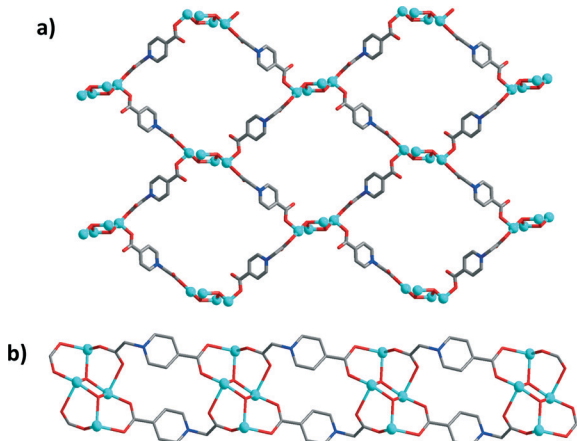


Fig. 3 (a) View of the 2D grid structure of **1** with a (4,4) topology. The blue balls represent Cu(II) ions. (b) View of the 1D chain of **1**, showing the linking fashion of the pillared double bridge with tetranuclear Cu(II) cores.

which is shorter than that in the 2D sheet (14.8961(73) Å). Thus, although each core possesses eight bridging L ligands sticking out for intercore connection, it actually connects six others and serves as a 6-connected octahedral node. Based on the above analysis, the 3D structure can be considered as being constructed from 2D rhombus-gird layers pillared by bis-bidentate μ_4 -bridging ligands. Obviously, the overall topology of the 3D framework is best described as a tilted α -Po type framework based on three intersecting (4,4) nets (Fig. 4).²¹ In contrast, the same tetranuclear $[\text{Cu}_4(\mu_3\text{-OH})_2]^{6+}$ core enveloped by eight same L ligands in the compound $[\text{Cu}_4(\text{L})_4(\text{OH})_2(\text{H}_2\text{O})_2]\text{[NO}_3\text{]}_2 \cdot 3\text{H}_2\text{O}$ acts as a 6-connected hexagonal node rather than an octahedral node, leading to a (3,6) topological 2D network, which arise from the anion effect.¹⁰ Additionally, as observed in the similar compounds, large voids were formed in the 3D framework, which accommodate vast guest water molecules, which further form a 2D layered water cluster *via* O–H···O hydrogen bonds since the adjacent O···O distances are in the range of 2.42–3.08 Å, although the water H atoms could not be found (ESI, Table S1 and Fig. S1†).²² After removal of these guest water molecules in the voids, the effective free volume is approximately 27.6% (679.9 Å³ out of the 2460.0 Å³ per unit cell volume) by Platon.²³

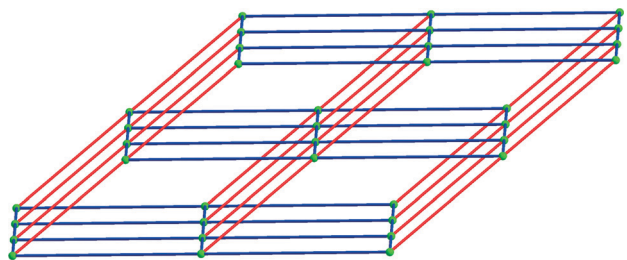


Fig. 4 A schematic representation of the 3D-frame architecture of **1** (green ball: tetranuclear Cu(II) node).

Structure of $[\text{Ag}_2(\text{L})(\text{NO}_3)] \cdot \text{H}_2\text{O}$ (2)

Silver salts tend to generate multinuclear clusters in the construction of coordination polymers with carboxylate ligands, and the Ag(I) ion usually displays versatile and irregular coordination geometries, being in favour of the formation of a distinct structure.²⁴ As anticipated, complex **2** displays a unique double-layered structure consisting of 2D sheets pillared by nitrate anions. Compared with **1**, compound **2** also belongs to the monoclinic $P2_1/n$ space group. Its asymmetric unit consists of two independent Ag(I) ions, one L ligand and one nitrate anion, as well as one lattice water molecule. As depicted in Fig. 5, each Ag1 ion is triangularly coordinated by three O atoms from two L ligands and one nitrate anion with bond angles around Ag1 in the range of 88.21(12)° to 136.23(13)°, whereas Ag2 is located in an irregular tetragonal pyramid of oxygen atoms from four different L ligands and one nitrate anion. The bond distances and angles around Ag2 are presented in Table 2. The Ag1 and Ag2 ions are bis(carboxylate-O,O')-bridged to give rise to a dinuclear $[\text{Ag}_2(\text{O}_2\text{CR})_2]$ unit with a Ag···Ag distance of 2.8367(6) Å, which is shorter than that (2.89 Å) in the metallic Ag and implies the existence of strong Ag–Ag interaction in **2**.²⁵ Such $[\text{Ag}_2(\text{O}_2\text{CR})_2]$ units are joined together *via* L ligands with a head-to-tail arrangement to generate a 1D chain, which are further extended into a 2D cationic network *via* the linkage of Ag2 with O3B from the adjacent dimer [Ag₂–O3B 2.382(3) Å] (Fig. 6a). Additionally, the distance of Ag2–Ag1A is 3.2073(6) Å, being shorter than twice the van der Waals radius of silver ions (3.44 Å), which implies the presence of argentophilic interactions, since the upper limit for Ag–Ag contact in silver(I) complexes is estimated as 3.30 Å.²⁶ Obviously, the Ag–Ag interactions assemble the adjacent Ag(I) ions into the 1D zigzag silver chain running parallel to the *b* axis. Intriguingly, two centrosymmetric cationic 2D layers are pillared by the counter nitrate anion *via* the Ag–O coordination interaction, resulting in a rare double-layered structure with 1D channels side by side (Fig. 6b), in which the solvated water molecules are stabilized and connected into a 1D chain *via* O–H···O hydrogen bonds with O···O distances ranging from 3.076(6) to 3.183(7) Å (ESI, Table S1†). According to the simplification principle, the resulting structure of **2** is a 3-nodal net with a point (Schläfli) symbol of {4¹⁰·6¹¹} {4³} {4⁴·6²}.

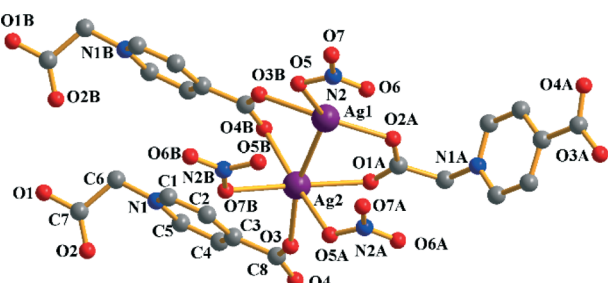


Fig. 5 The coordination environment of Ag(I) ions in **2** with numbering atoms, in which the hydrogen atoms and water molecules were omitted for clarity.

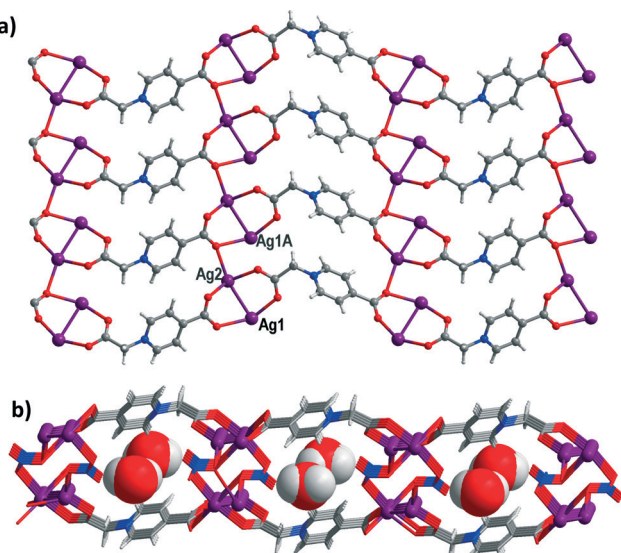


Fig. 6 (a) 2D network of **2**. All the guest water molecules were omitted for clarity. (b) 2D double-layered structure of **2** containing 1D channels along the *b* axis occupied by water molecules.

Structure of $[\text{Pb}(\text{L})(\text{NO}_3)]$ (**3**)

When post-transition metal ion $\text{Pb}(\text{II})$ with an identifiable void for ligand disposition (namely, inert-pair effect²⁷) is utilized, an intriguing 2D chiral network **3** is obtained. Colorless crystals of the title complex **3** were obtained by the liquid-phase diffusion method rather than the vapour-phase diffusion method used in **1**. The X-ray structure analysis revealed that **3** crystallizes in the orthorhombic system with chiral orthorhombic space group $P2_12_12_1$, implying that the complex underwent conglomerate crystallization. As depicted in Fig. 7, each $\text{Pb}(\text{II})$ center coordinates to four carboxyl oxygen atoms from four different L ligands and one nitrate anion, showing a hemidirected geometry. That is, there is an identifiable gap in the coordination sphere, implying the presence of a stereo-chemically active electron lone pair on the $\text{Pb}(\text{II})$ center.²⁸ The $\text{Pb}-\text{O}$ bond lengths vary from 2.437(5) to 2.692(8) Å, and $\text{O}-\text{Pb}-\text{O}$ bond angles are in the range of 75.0(2) $^\circ$ –155.8(2) $^\circ$ as listed in Table 2, in which the $\text{Pb}_1-\text{O}_2\text{B}$ bond length (2.437(5) Å) is shorter than those from the other four $\text{Pb}-\text{O}$ bond lengths, which suggests that the site of the lone pair electron lies in the opposite side of the shortest $\text{Pb}_1-\text{O}_2\text{B}$ bond.^{27,29}

The most peculiar structural feature of **3** is the assembly of homo-chiral 2_1 helices, affording a chiral 2D polymeric network. As depicted in Fig. 8, the L ligand serves as a bis-bidentate μ_4 -bridging ligand, in which two carboxyl groups adopt the same $\mu_2\kappa^1\text{O}\cdots\kappa^1\text{O}'$ bridging mode to link two $\text{Pb}(\text{II})$ ions. While one carboxyl group takes the syn-skew coordination mode, the other adopts the skew-skew coordination mode. In turn, each $\text{Pb}(\text{II})$ ion links two L ligands running parallel to the *b* axis, leading to the formation of a 1D single-stranded right-handed helix with a repeating period of 11.32 Å (Fig. 8b). The 1D spiral chains lock together through the

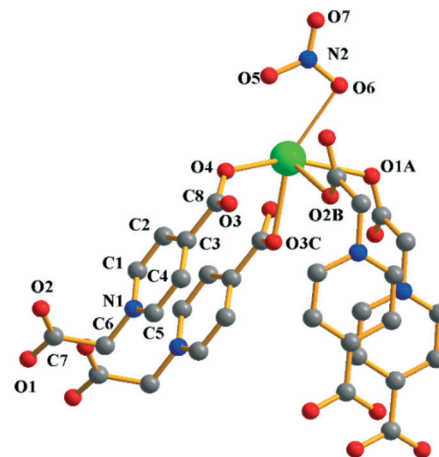


Fig. 7 The coordination environment of $\text{Pb}(\text{II})$ centres in **3**. The hydrogen atoms are omitted for clarity.

sharing of $\text{Pb}(\text{II})$ ions to form a novel 2D network in the *ab* plane. In other words, each $\text{Pb}(\text{II})$ center links four twisting L ligands along two diagonal directions of the rhombus, producing a corrugated 2D cationic layer (Fig. 8a). Topologically, each $\text{Pb}(\text{II})$ ion and L ligand can be both regarded as a 4-connected node, resulting in a ML type binodal $(4,4)$ -connected sql net with a point (Schläfli) symbol of $\{4^4 \cdot 6^2\}\{4^4 \cdot 6^2\}$. It is worth noting that the adjacent two 2D layers have the same chirality with opposite oriented helices, which are further held together via $\text{Pb}\cdots\text{O}_{\text{nitrate}}$ interactions with the distance ranging from 2.69 to 2.82 Å, as well as $\text{C}-\text{H}\cdots\text{O}$ hydrogen bonding interactions with $\text{C}\cdots\text{O}$ distances in the range of 2.86–3.29 Å to form a 3D framework structure (Fig. 9).

Structure of $[\text{Pb}_3(\text{L})_4\text{Br}_2(\text{H}_2\text{O})_2]$ (**4**)

Compared with **3**, $\text{Pb}(\text{II})$ complex **4** has a different structure, which was obtained by the reaction of the L ligand with $\text{Pb}(\text{NO}_3)_2 \cdot 4\text{H}_2\text{O}$, as well as KBr. In contrast to the 2D layered structure of **3**, **4** exhibits a 3D plywood-like structure consisting of two types of 1D chains, in which the bromide anions take part in the coordination. Structure analysis

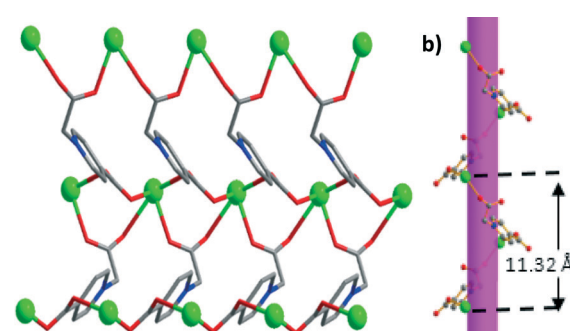


Fig. 8 (a) Side view of the 1D helical chain of **3** along the *b* axis. (b) The wavelike chiral 2D cationic network, in which the hydrogen atoms and nitrate anions were omitted for clarity.

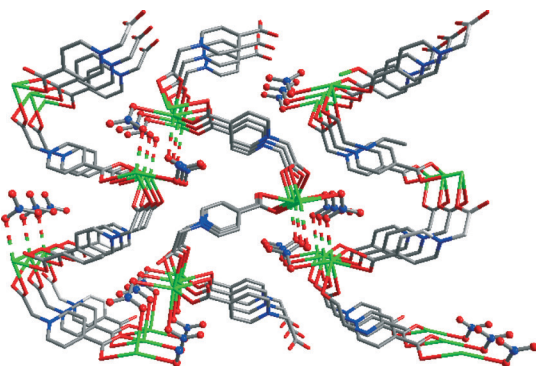


Fig. 9 The packing diagram with weak $\text{Ag}\cdots\text{O}$ interactions indicated by dotted lines, showing the same chirality of neighboring layers.

reveals that the repeating unit of 3 is made up of one and a half $\text{Pb}(\text{II})$ ions, two L ligands, one bromide anion, as well as one guest water molecule. The Pb1 ion is bound to four independent L ligands (Pb1-O distances, $2.637(10)$ – 2.9175 (13) Å) and two bromide anions, furnishing a rare triangular prism geometry as illustrated in Fig. 10. In contrast to Pb1 , the hexa-coordinated Pb2 ion is surrounded with four L ligands (Pb-O distances, $2.515(11)$ – $2.713(9)$ Å) and one terminal water molecule (Pb-O distance, $2.693(11)$ Å), providing an approximate tetragonal-pyramidal coordination environment if the chelating carboxyl group was regarded as one coordination site. Based on the above analysis, two hexa-coordinated $\text{Pb}(\text{II})$ centers with different coordination environments can both be regarded as 4-connected nodes. Conversely, two L ligands both serve as a 3-connected organic linker, which result in a 3:4 M:L ratio, consistent with the experimental formula. Compared with 3, two types of μ_3 -bridging L ligands take different coordination modes. The carboxyl groups of one L ligand take the $\mu_1\kappa^1\text{O}$ and $\mu_2\kappa^1\text{O}\cdot\kappa^1\text{O}'$ coordination

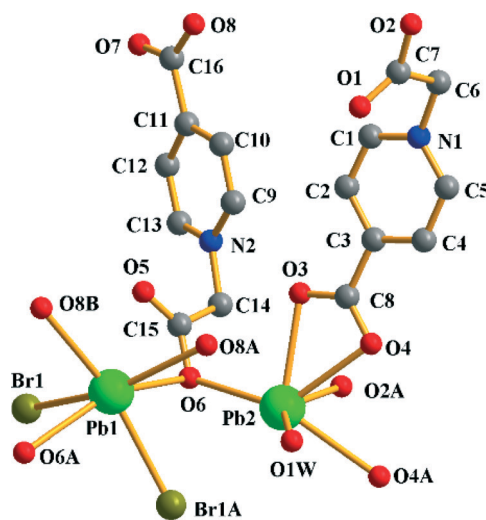


Fig. 10 View of 4 showing the coordination environment around the $\text{Pb}(\text{II})$ centers.

modes, and the carboxyl groups of the other adopt $\mu_2\kappa^1\text{O}$ and $\mu_1\kappa^1\text{O}$ coordination modes, respectively. As illustrated in Fig. 11a, two Pb1 ions and two L-shaped L ligands first form a M_2L_2 twenty-membered metallocycle, which further afford an infinite 1D beaded chain by sharing of Pb1 ions in an $\cdots\text{ABAB}\cdots$ repeating fashion along the c axis. At the same time, two Pb2 ions and two L ligands also first form a M_2L_2 twenty-membered metallocyclic ring, which further extend an infinite 1D chain along the b axis via Pb2-O coordination interaction (Fig. 11b). Then, the former chains connecting with the latter in a cross-like arrangement via Pb2-O coordination produce a rare 3D plywood-like structure with a new $\{3^2\cdot4^3\cdot6\cdot8^6\cdot10^3\}_2\{3^2\cdot4^4\}_2\{3^4\cdot4^2\cdot8\cdot9^4\cdot10^4\}\{4^2\cdot6\}_2$ topology (Fig. 12).³⁰

Structure of $[\text{Pr}(\text{L})_2(\text{H}_2\text{O})_2(\text{NO}_3)]$ (5)

Rare earth ions have a large ionic radius, along with a greater coordination number. Structure analysis reveals that complex 5 features a 3D dia-net structure with 3-fold interpenetration, whose fundamental unit is composed of a half $\text{Pr}(\text{III})$ ion, one L ligand, a half nitrate anion and one coordinated water molecule. The $\text{Pr}(\text{III})$ center adopts a distorted pentagonal-bipyramidal geometry with a O_8 donor set, regarding the chelating nitrate anion as one coordination site, and is bound to four independent L ligands, two terminal water molecules and one chelate nitrate anion (Fig. 13). Among them, two water molecules occupy two vertices with a Pr-O distance of $2.446(3)$ Å. Regardless of terminal water molecules and nitrate anions, the $\text{Pr}(\text{III})$ center indeed acts as a 4-connected node to link four L ligands. At the same time, the L ligand serves as a bis-monodentate bridging mode to connect two 4-connected $\text{Pr}(\text{III})$ centers to form a diamondoid 3D architecture with a $\text{Pr}\cdots\text{Pr}$ distance of $12.3026(6)$ Å (Fig. 14). Because of the spacious nature of the single network, the 3D framework has a large vacancy to allow not only the presence of coordinated water molecules and nitrate anions, but also the inclusion of another two 3D frameworks. Therefore, the most salient structure feature of 5 is 3-fold interpenetration of the 3D diamondoid framework (Fig. 15).

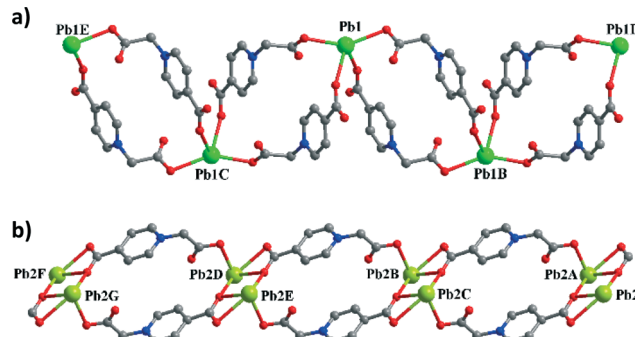


Fig. 11 (a) View of the 1D infinite chain structure consisting of Pb1 and the L ligand in 4. (b) View of the 1D infinite chain structure consisting of Pb2 and the L ligand in 4.

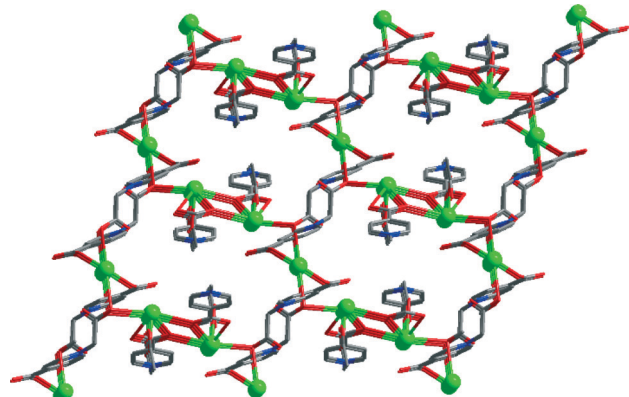


Fig. 12 Representation of the cross-like arrangement of two types of 1D chains to generate a 3D plywood-like array in 4.

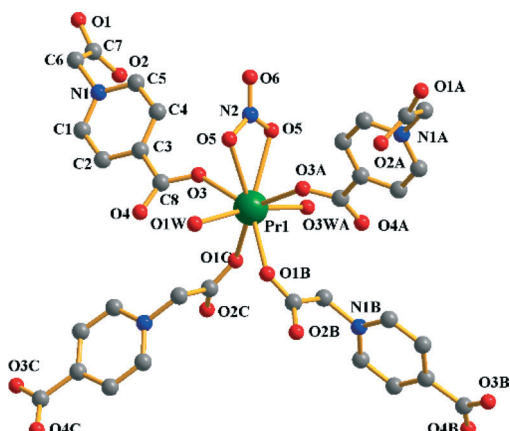


Fig. 13 The local coordination environment of the Pr(III) center in 5, in which the hydrogen atoms were omitted for clarity.

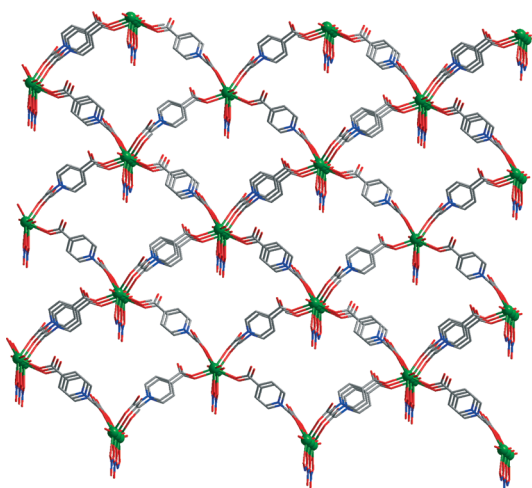


Fig. 14 The wire drawing of 5 with diamondoid nets.

The effects of ligand L on the structures of target complexes

Based on the above descriptions, we explicitly realize that the ligand L adopting different coordination modes plays crucial

roles in determining the final structure of the targeted product. Additionally, the tiny conformational variation of semirigid ligand L, behaving differently when binding to different metal centers, also has a subtle influence. For further structural analysis, detailed data analysis of semirigid ligand L in 1–5 is listed in Table 3 and Scheme 2. Obviously, the dihedral angles between the planes defined by carboxylic methyl and N-methylene pyridine, respectively, fall into the broad range of 67.09° – 84.33° . In the case of 1, the L ligands, adopting bis-monodentate or bis-bidentate modes (mode I and II), both connect two tetrานuclear Cu(n) clusters, leading to an α -Po type 3D framework. At the same time, the difference of two dihedral angles is 15.77° , implying the occurrence of obvious rotation with carboxylic methyl. In contrast to 1, there is only one type of L ligand in 2, which links five Ag(I) ions in mode III to form a 2D network with a dihedral angle of 67.09° , pillared by nitrate anions to generate a novel double-layered structure with 1D channels. Just like 2, in the case of 3, only one type of L ligand exists with a bigger dihedral angle of 84.33° than that of 2, but notably, both carboxylic groups take rare non-coplanar (syn-skew) bridging mode IV rather than common coplanar (syn-syn) mode II. In the case of 4, the coordination modes of two types of L ligands are apparently distinct with similar dihedral angles (81.09° and 76.50°), adopting $\mu_{3-k}^1 O : k^1 O' : k^2 O', O''$ and $\mu_{3-2k}^1 O : k^1 O'$ bridging fashions (mode V and mode VI), although both ligands serve as a 3-connected linker. It is worth noting that the carboxylic methyl in mode VI takes a rare mono-oxygen atomic (syn-skew) bridging mode. In 5, the only L ligand acts in a (syn-anti) bis-monodentate bridging fashion in mode VII with a dihedral angle of 78.92° to join with the distorted tetrahedral 4-connected Pr(m) node, leading to a 3-fold interpenetrating diamondoid network. According to the above-mentioned analysis, we conclude that the semirigid L ligand can timely fine tune its conformation to adapt the coordination geometry of metal centers, leading to the structural diversity of targeted products.

FT-IR spectroscopy analyses

The IR spectra of compounds 1–5 are similar (ESI, Fig. S2†). In the IR spectra of 1, 2, 4 and 5, the broad bands at 3650–3180 cm^{−1} indicate the presence of guest or coordinated water molecules and the existence of hydrogen bonding interactions, in agreement with their crystal structures. The

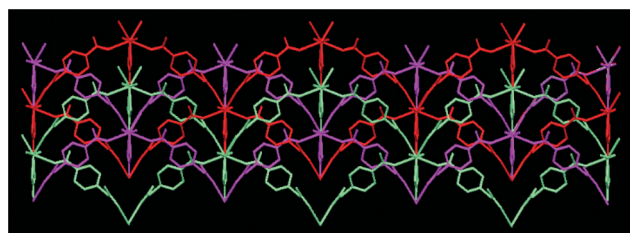


Fig. 15 The threefold interpenetrating diamondoid framework in 5.

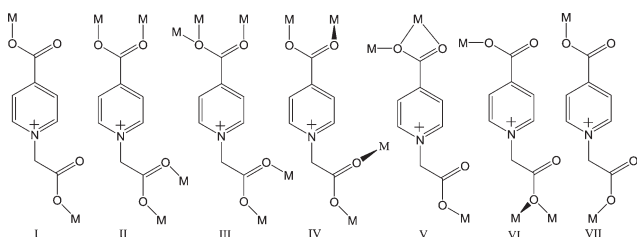
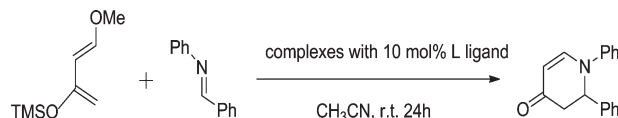
Table 3 The structure parameters of the L ligand in complexes 1–5

| Complexes | Coordination modes | Bridging fashion | Dihedral angles (°) |
|-----------|--------------------|---|---------------------|
| 1 | Mode I | $\mu_2\kappa^1O:\kappa^1O'$ | 83.31 |
| | Mode II | $\mu_4\kappa^1O:\kappa^1O':\kappa^1O'':\kappa^1O'''$ | 67.54 |
| 2 | Mode III | $\mu_5\kappa^1O:\kappa^1O':2\kappa^1O'':\kappa^1O'''$ | 67.09 |
| | Mode IV | $\mu_4\kappa^1O:\kappa^1O':\kappa^1O'':\kappa^1O'''$ | 84.33 |
| 3 | Mode V | $\mu_3\kappa^1O:\kappa^1O':\kappa^2O',O''$ | 81.09 |
| | Mode VI | $\mu_3\kappa^1O:\kappa^1O'$ | 76.50 |
| 5 | Mode VII | $\mu_2\kappa^1O:\kappa^1O'$ | 78.92 |

absence of the characteristic bands in the range of 1730–1680 cm⁻¹ indicates the complete deprotonation of ligand L.³¹ The bands of asymmetric and symmetric stretching vibration of carboxyl groups appear in the range of 1665–1570 cm⁻¹ and 1430–1315 cm⁻¹, respectively. The splitting of $\nu_{as}(\text{COO})$ and $\nu_s(\text{COO})$ suggests that the carboxylate groups of ligand L take different coordination modes. In addition, the spectra of 1–5 show medium intensity bands at about 3050 cm⁻¹, which are attributed to the stretching vibration of aromatic C–H bonds. All these facts are highly consistent with the single crystal X-ray diffraction results.

Thermogravimetric analyses

In order to evaluate the thermal stability, thermogravimetric analyses (TGA) of complexes 1–5 were carried out under flowing N₂ atmosphere with a heating rate of 10 °C min⁻¹ in the temperature range of 30 to 800 °C (ESI, Fig. S3†). For 1, the first weight loss of 15.78% from 30 to 166 °C corresponds to the loss of guest water molecules (calcd 16.15 %), and then the framework began to decompose gradually. For 2, a total weight loss of 3.65% was observed in the temperature region of 30–178.5 °C, corresponding to the removal of lattice water molecules (expected 3.78%), and above this temperature, the compound started to decompose rapidly. In the case of 3, the TGA result shows that the samples of 3 were stable up to 195 °C, and above this temperature, it starts to lose mass rapidly. In contrast to lead(II) complex 3, the lead(II) complex 4 begins to lose weight slowly from the starting temperature 30 °C up to the similar temperature 195 °C like that in 3 with a weight loss of 2.41%, which is in agreement with the departure of two coordinated water molecules (calcd 2.34%), and further rapid weight loss was observed in the temperature range of 195–254 °C. As to 5, it is worth noting that the gradual weight

**Scheme 2** The coordination modes of the L ligand in 1–5.**Scheme 3** Aza-Diels–Alder reaction of *N*-benzylideneaniline and Danishefsky's diene catalysed by complexes 1–5 in dry CH₃CN.

loss corresponding to coordinated water molecules (calcd 3.00%) was not observed before 179 °C, above which the samples begin to decompose rapidly. This phenomenon may be attributed to the coexistence of strong hydrogen bonding interactions and coordination interaction.³²

Nonlinear optical properties

Compounds 3 and 5 crystallized as clear, colorless crystals in the acentric space group *P*1, and *Fdd*2, respectively, so Kurtz powder SHG measurements were performed on 3 and 5 to confirm their acentricity and to further evaluate their potential as a second-order NLO material. In order to ensure the purity of the samples, the experimental PXRD patterns of 3 and 5 were first tested and compared with their simulated ones (ESI, Fig. S4†). The results reveal that the experimental peak positions agree well with the simulated ones, indicating the products have been successfully obtained as pure crystalline phases. Approximate estimation was carried out by the Kurtz powder second harmonic generation (SHG) measurements ($\lambda = 1064$ nm). Comparison of the results with those obtained for urea was obtained from a powdered sample (80–150 μm diameter) in the form of a pellet. The result showed that the compounds are SHG active with a response of about 0.8 and 0.5 times of the urea, respectively.

The aza-Diels–Alder reaction catalysed by complexes 1–5

As shown in Scheme 3, complexes 1–5 were tested as catalysts in the aza-Diels–Alder reaction of *N*-benzylideneaniline and Danishefsky's diene. The reactions were carried out for 24 h at room temperature in dry acetonitrile and the results are given in Table 4. Complexes 2 with a 2D structure gave yields of 17%, while 3D complexes 1 and 5 with large cavity led to moderate yields of 34% and 41%, respectively. Interestingly, two Pb(II) complexes 3 and 4 were superior to the above-mentioned three compounds affording the expected product 2,3-dihydro-1,2-diphenylpyridin-4(1H)-one with relatively high

Table 4 Aza-Diels–Alder reaction of *N*-benzylideneaniline and Danishefsky's diene catalysed by complexes 1–5 in dry CH₃CN^a

| Entry | Complexes | Yield ^b (%) |
|-------|-----------|------------------------|
| 1 | 1 | 34 |
| 2 | 2 | 17 |
| 3 | 3 | 51 |
| 4 | 4 | 70 |
| 5 | 5 | 41 |

^a See Experimental for details. ^b Isolated yields.

yields of 51% and 70%. The results imply that all complexes 1–5 with weak Lewis acidity in the pyridinium unit can act as catalysts in the aza-Diels–Alder reaction and the structures have a subtle influence on the catalytic effect.

Conclusions

In conclusion, we have successfully synthesized and characterized five new coordination polymers based on L-shaped semirigid ligand 1-carboxymethylpyridinium-4-carboxylate (L) by utilizing various metal salts. Complexes 1, 4 and 5 have 3D structures, whereas 2 and 3 exhibit different 2D layered architectures. In contrast to complexes 3–5 with a monomer metal node, complexes 1 and 2 use tetranuclear Cu(II) and dinuclear Ag(I) as the nodes with distorted octahedral and linear geometries, respectively. It is worth noting that 5 possesses 3-fold interpenetrating structures. Moreover, complexes 3 and 5 crystallize with acentric space groups *P*1 and *Fdd*2, which are SHG active with modest powder SHG intensity. Based on the Lewis acidity of the pyridinium unit of ligand L, complexes 1–5 were used as catalysts for aza-Diels–Alder reaction with moderate yield. The results demonstrate that the careful selection of the organic linker is helpful for the rational design and construction of the coordination polymer.

Acknowledgements

This work was financially supported by the National Natural Science Foundation of China (grant no. 21201111) and the Domestic Visiting Scholars Program of Yong Key Teachers from Colleges and Universities in Shandong Province.

References

- 1 C. Wang, T. Zhang and W. Lin, *Chem. Rev.*, 2012, **112**, 1084; Z. Hulvey, E. Ayala, J. D. Furman, P. M. Forster and A. K. Cheetham, *Cryst. Growth Des.*, 2009, **9**, 4759; Q. Ye, Y.-H. Li, Q. Wu, Y.-M. Song, J.-X. Wang, H. Zhao, R.-G. Xiong and Z. Xue, *Chem. – Eur. J.*, 2005, **11**, 988.
- 2 J. Heine and K. Müller-Buschbaum, *Chem. Soc. Rev.*, 2013, **42**, 9232; P. Wang, J.-P. Ma and Y.-B. Dong, *Chem. – Eur. J.*, 2009, **15**, 10432; C. Yan, L. Chen, R. Feng, F. Jiang and M. Hong, *CrystEngComm*, 2009, **11**, 2529; X. Li, H.-L. Sun, X.-S. Wu, X. Qiu and M. Du, *Inorg. Chem.*, 2010, **49**, 1865.
- 3 S. Ma and H.-C. Zhou, *Chem. Commun.*, 2010, **46**, 44; Z. Xiang, D. Cao, J. Lan, W. Wang and D. P. Broom, *Energy Environ. Sci.*, 2010, **3**, 1469; B. Xiao, P. J. Byrne, P. S. Wheatley, D. S. Wragg, X. Zhao, A. J. Fletcher, K. M. Thomas, L. Peters, J. S. O. Evans, J. E. Warren, W. Zhou and R. E. Morris, *Nat. Chem.*, 2009, **1**, 289; S. Ma and H.-C. Zhou, *J. Am. Chem. Soc.*, 2006, **128**, 11734; S. Ma, D. Yuan, X.-S. Wang and H.-C. Zhou, *Inorg. Chem.*, 2009, **48**, 2072.
- 4 Y.-S. Bae and R. Snurr, *Angew. Chem., Int. Ed.*, 2011, **50**, 11586; Q. Yang, D. Liu, C. Zhong and J.-R. Li, *Chem. Rev.*, 2013, **113**, 8261; Y. Liu, W. Xuan and Y. Cui, *Adv. Mater.*, 2010, **22**, 4112; J.-R. Li, Y. Ma, M. C. McCarthy, J. Sculley, J. Yu, H.-K. Jeong, P. B. Balbuena and H.-C. Zhou, *Coord. Chem. Rev.*, 2011, **255**, 1791; Y.-S. Bae and R. Snurr, *Angew. Chem., Int. Ed.*, 2011, **50**, 11586.
- 5 K. K. Tanabe and S. M. Cohen, *Angew. Chem., Int. Ed.*, 2009, **48**, 7424; Y. Liu, W. Xuan and Y. Cui, *Adv. Mater.*, 2010, **22**, 4112; A. Corma, H. García and F. X. L. i. Xamena, *Chem. Rev.*, 2010, **110**, 4606; X.-M. Lin, T.-Y. Li, L.-F. Chen, L. Zhang and C.-Y. Su, *Dalton Trans.*, 2012, **41**, 10422; K. Mo, Y. Yan and Y. Cui, *J. Am. Chem. Soc.*, 2014, **136**, 1746; D. N. Dybtsev, A. L. Nuzhdin, H. Chun, K. P. Bryliakov, E. P. Talsi, V. P. Fedin and K. Kim, *Angew. Chem., Int. Ed.*, 2006, **45**, 916; Y.-Z. Chen, Y.-X. Zhou, H. Wang, J. Lu, T. Uchida, Q. Xu, S.-H. Yu and H.-L. Jiang, *ACS Catal.*, 2015, **5**, 2062; Y.-X. Zhou, Y.-Z. Chen, Y. Hu, G. Huang, S.-H. Yu and H.-L. Jiang, *Chem. – Eur. J.*, 2014, **20**, 14976.
- 6 Y. Ikezoe, G. Washino, T. Uemura, S. Kitagawa and H. Matsui, *Nat. Mater.*, 2012, **11**, 1081; M. Meilikov, S. Furukawa, K. Hirai, R. A. Fischer and S. Kitagawa, *Angew. Chem., Int. Ed.*, 2013, **52**, 341; S.-D. Han, Y.-Q. Chen, J.-P. Zhao, S.-J. Liu, X.-H. Miao, T.-L. Hu and X.-H. Bu, *CrystEngComm*, 2014, **16**, 753.
- 7 T. R. Cook, Y.-R. Zheng and P. J. Stang, *Chem. Rev.*, 2013, **113**, 734; M. Eddaoudi, D. B. Moler, H. Li, B. Chen, T. M. Reineke, M. O’Keeffe and O. M. Yaghi, *Acc. Chem. Res.*, 2001, **34**, 319; O. K. Farha and J. T. Hupp, *Acc. Chem. Res.*, 2010, **43**, 1166; F. A. A. Paz, J. Klinowski, S. M. F. Vilela, J. P. C. Tomé, J. A. S. Cavaleiro and J. Rocha, *Chem. Soc. Rev.*, 2012, **41**, 1088; T. Yamada, K. Otsubo, R. Makiura and H. Kitagawa, *Chem. Soc. Rev.*, 2013, **42**, 6655; G. Kumar and R. Gupta, *Chem. Soc. Rev.*, 2013, **42**, 9403.
- 8 Y. Li, X. Meng, L. Cao, Y. Wang, G. Yin, M. Gao, L. Wen and A. Wu, *Cryst. Growth Des.*, 2008, **8**, 1645; W. Yang, M. Guo, F.-Y. Yi and Z.-M. Sun, *Cryst. Growth Des.*, 2012, **12**, 5529; J. Zhang, Y.-S. Xue, J. Bai, M. Fang, Y.-Z. Li, H.-B. Du and X.-Z. You, *CrystEngComm*, 2011, **13**, 6010; C.-L. Yi, Y. Tang, W.-S. Liu and M.-Y. Tan, *Inorg. Chem. Commun.*, 2007, **10**, 1505.
- 9 C. N. R. Rao, S. Natarajan and R. Vaidhyanathan, *Angew. Chem., Int. Ed.*, 2004, **43**, 1466; W. Lu, D. Yuan, T. A. Makal, J.-R. Li and H.-C. Zhou, *Angew. Chem., Int. Ed.*, 2012, **51**, 1580; J.-Y. Wu, M.-T. Ding, Y.-S. Wen, Y.-H. Liu and K.-L. Lu, *Chem. – Eur. J.*, 2009, **15**, 3604; M.-L. Hu, A. Morsali and L. Aboutorabi, *Coord. Chem. Rev.*, 2011, **255**, 2821.
- 10 Y.-Q. Huang, H.-D. Cheng, B.-L. Guo, Y. Wan, H.-Y. Chen, Y.-K. Li and Y. Zhao, *Inorg. Chim. Acta*, 2014, **421**, 318; Y.-Q. Huang, Q. Zhao, Y.-H. Wang, S.-S. Ge and Q. Shao, *J. Chem. Crystallogr.*, 2012, **42**, 706; G.-Q. Kong and C.-D. Wu, *CrystEngComm*, 2012, **14**, 847; Y.-Q. Wang, A.-L. Cheng, P.-P. Liu and E.-Q. Gao, *Chem. Commun.*, 2013, **49**, 6995; Y.-Q. Wang, K. Wang, Q. Sun, H. Tian, E.-Q. Gao and Y. Song, *Dalton Trans.*, 2009, 9854.
- 11 M. Higuchi, K. Nakamura, S. Horike, Y. Hijikata, N. Yanai, T. Fukushima, J. Kim, K. Kato, M. Takata, D. Watanabe, S. Oshima and S. Kitagawa, *Angew. Chem., Int. Ed.*, 2012, **51**, 8369; M. Higuchi, D. Tanaka, S. Horike, H. Sakamoto, K. Nakamura, Y. Takashima, Y. Hijikata, N. Yanai, J. Kim, K.

- Kato, Y. Kubota, M. Takata and S. Kitagawa, *J. Am. Chem. Soc.*, 2009, **131**, 10336; V. Jurčík and R. Wilhelm, *Org. Biomol. Chem.*, 2005, **3**, 239.
- 12 X.-B. Wang, J.-E. Dacres, X. Yang, K.-M. Broadus, L. Lis, L.-S. Wang and S. R. Kass, *J. Am. Chem. Soc.*, 2003, **125**, 296.
- 13 P. R. Edgington, P. McCabe, C. F. Macrae, E. Pidcock, G. P. Shields, R. Taylor, M. Towler and J. V. D. Streek, *J. Appl. Crystallogr.*, 2006, **39**, 453.
- 14 G. M. Sheldrick, *SADABS, Program for Empirical Absorption Correction of Area Detector Data*, University of Göttingen, Germany, 1996.
- 15 Agilent, *CrysAlis PRO*, Agilent Technologies Ltd, Yarnton, Oxfordshire, England, 2011.
- 16 G. M. Sheldrick, *SHELX-97, An Integrated System for Solving Crystal Structures from Diffraction Data*, University of Göttingen, Germany, 1997.
- 17 G. M. Sheldrick, *SHELX-97, An Integrated System for Refining Crystal Structures from Diffraction Data*, University of Göttingen, Germany, 1997.
- 18 G. M. Sheldrick, *SHELXTL Version 6.10*, Bruker AXS Inc., Madison, Wisconsin, USA, 2000.
- 19 A. W. Addison, T. N. Rao, J. Reedijk, J. V. Rijn and G. C. Verschoor, *J. Chem. Soc., Dalton Trans.*, 1984, 1349.
- 20 Y. Q. Zhang and J. L. Lin, *Z. Anorg. Allg. Chem.*, 2002, **628**, 203.
- 21 R. Haldar and Y. K. Maji, *CrystEngComm*, 2012, **14**, 685; V. S. S. Kumar, F. C. Pigge and N. P. Rath, *New J. Chem.*, 2004, **28**, 1192; Y.-T. Yang, Q. Zhao, C.-Z. Tu, F.-X. Cheng and F. Wang, *Inorg. Chem. Commun.*, 2014, **40**, 43; S. Mohapatra, K. P. S. S. Hembram, U. Waghmare and T. K. Maji, *Chem. Mater.*, 2009, **21**, 5406; T. Li, X.-H. Huang, Y.-F. Zhao, H.-H. Li, S.-T. Wu and C.-C. Huang, *Dalton Trans.*, 2012, **41**, 12872.
- 22 T. F. Mastropietro, D. Armentano and G. D. Munno, *Polyhedron*, 2009, **28**, 2965; S.-M. Chen and T.-T. Lian, *Inorg. Chem. Commun.*, 2010, **13**, 1380; L. Cheng, J.-B. Lin, J.-Z. Gong, A.-P. Sun, B.-H. Ye and X.-M. Chen, *Cryst. Growth Des.*, 2006, **6**, 2739; Y.-Q. Huang, Z.-L. Shen, T.-A. Okamura, Y. Wang, X.-F. Wang, W.-Y. Sun, J.-Q. Yu and N. Ueyama, *Dalton Trans.*, 2008, 204.
- 23 A. L. Spek, *PLATON, A Multipurpose Crystallographic Tool*, Utrecht University, Utrecht, The Netherlands, 2001.
- 24 J.-P. Zhang, Y.-Y. Lin, W.-X. Zhang and X.-M. Chen, *J. Am. Chem. Soc.*, 2005, **127**, 14162; S. Hiraoka, K. Harano, T. Tanaka, M. Shiro and M. Shionoya, *Angew. Chem., Int. Ed.*, 2003, **42**, 5182; T. Nakamura, H. Ube and M. Shionoya, *Angew. Chem., Int. Ed.*, 2013, **52**, 12096; G. Yang and R. G. Raptis, *Chem. Commun.*, 2004, 2058.
- 25 M. Jansen, *Angew. Chem., Int. Ed. Engl.*, 1987, **26**, 1098; K. Singh, J. R. Long and P. J. Stavropoulos, *J. Am. Chem. Soc.*, 1997, **119**, 2942; J. Xie, Y. Q. Huang, T. A. Okamura, W. Y. Sun and N. Ueyama, *Z. Anorg. Allg. Chem.*, 2007, **633**, 1211.
- 26 A. L. Goodwin, M. Calleja, M. J. Conterio, M. T. Dove, J. S. O. Evans, D. A. Keen, L. Peters and M. G. Tucker, *Science*, 2008, **319**, 794; E. Soyer, F. Yilmaz, V. T. Yilmaz, O. Buyukgungor and W. T. A. Harrison, *J. Inorg. Organomet. Polym.*, 2010, **20**, 320.
- 27 C.-P. Li, J. Chen and M. Du, *CrystEngComm*, 2010, **12**, 4392; L. Shimoni-Livny, J. P. Glusker and C. W. Bock, *Inorg. Chem.*, 1998, **37**, 1853; D. R. McKeney, *J. Chem. Educ.*, 1983, **60**, 112.
- 28 C. Janiak, S. Temizdemir, T. G. Scharmann, A. Schmalstieg and J. Demtschuk, *Z. Anorg. Allg. Chem.*, 2000, **626**, 2053; J. H. Thurston, C. G.-Z. Tang, D. W. Trahan and K. H. Whitmire, *Inorg. Chem.*, 2004, **43**, 2708.
- 29 G. Malandrino, R. L. Nigro, P. Rossi, P. Dapporto and I. L. Fragalà, *Inorg. Chim. Acta*, 2004, **357**, 3927.
- 30 X.-Q. Lü, Y.-Q. Qiao, J.-R. He, M. Pan, B.-S. Kang and C.-Y. Su, *Cryst. Growth Des.*, 2012, **12**, 5529; F. Robinson and M. J. Zaworotko, *J. Chem. Soc., Chem. Commun.*, 1995, 2413.
- 31 X.-C. Chai, Y.-Q. Sun, R. Lei, Y.-P. Chen, S. Zhang, Y.-N. Cao and H.-H. Zhang, *Cryst. Growth Des.*, 2010, **10**, 658.
- 32 J.-A. Hua, Y. Zhao, Q. Liu, D. Zhao, K. Chen and W.-Y. Sun, *CrystEngComm*, 2014, **16**, 7536.